Progress In Electromagnetics Research B, Vol. 94, 53–74, 2021

Enhancing Detection Performances of Nonhomogeneous Weibull Clutter by Knowledge Based Systems Exploitation

Abdellatif Rouabah[1, *], M'hamed Hamadouche[2], Djamel Teguig[1], and Hamza Zeraoula[3]

Abstract—This article aims to study the behavior of Constant False Alarm Rate (CFAR) detectors for a heterogeneous Weibull clutter and its derivatives. CFAR architectures based on exploitation of the Combined Environmental Knowledge Base (CEKB) have been proposed, called Knowledge Based Systems-Maximum Likelihood-CFAR (KBS-ML-CFAR) and KBS-Log-t-CFAR for nonhomogeneous Weibull clutter at general parameters. A CFAR architecture that uses Geographic Information System (GIS) as a Knowledge Base (KB), called KBS-Forward Automatic Order Selection Ordered Statistics-CFAR (KBS-FAOSOS-CFAR) has been proposed for special Weibull parameters. The performances of the proposed detectors have been studied and analyzed by conducting MATLAB simulations. The simulation results show that the KBS-CFAR based on CEKB outperforms the ML and Log-t-CFAR in terms of clutter edge detection capability in nonhomogeneous Weibull clutter case. Compared with other KB, this KBS-CFAR based on CEKB performs well to preserve the probability of false alarm (P_{fa}) at a desired constant value. For special Weibull parameters, the proposed KBS-FAOSOS-CFAR based on GIS performs better than KBS-Dynamic-CFAR and KBS-Adaptive Linear Combined-CFAR (KBS-ALC-CFAR) in severe interference case. CFAR techniques have been implemented on the ADSP (Advanced Digital Signal Processor) processing board, and the results have been evaluated and discussed.

1. INTRODUCTION

The field of radar detection has been developed considerably over the years, thanks to techniques that offer the radar's operator the ideal exploitation of detection equipments. The first radars use the classic detection technique. This technique requires the intervention of the operator for decision making, based on the amplitude of the received signal, visualized on PPI (Plan Position Indicator). In this case, the radar operator must compare the amplitude of the received signal with a fixed threshold. If the amplitude of the received signal is greater than the chosen threshold, then the hypothesis H_1 is declared, which means that a target is present in the radar coverage zone; otherwise, we declare the inverse hypothesis H_0. The received echoes, coming from space, not only are those reflected by the targets, but the nature of the environment also poses a big decision problem for the radar operator, because the noise generated by the nature of the environment is considered the main source of noise for the radar. If the noise power is too high, it leads to an increase in the amplitude of the displayed signal on the PPI screen, and we will then be faced with a false alarm situation. To overcome the problem posed by the fixed threshold, another detection technique, called adaptive detection or CFAR detection, has been developed by Finn [1]. The threshold estimated by this technique is adapted to the signal level while the false alarm rate is maintained at a fixe value. In the literature, various types of CFAR detectors have been suggested, each of which is appropriate for a certain operating environment [2–4]. Since the

Received 20 August 2021, Accepted 1 October 2021, Scheduled 20 October 2021
* Corresponding author: Abdellatif Rouabah (rouabaheliana@gmail.com).
[1] Laboratoire Télécommunications, École Militaire Polytechnique, Bordj El-Bahri, Algiers, Algeria. [2] LIMOSE Laboratory, Université de Boumerdès, Algeria. [3] Département Radar, Ecole supérieure-Ali Chabati, Réghaia, Algiers, Algeria.

detection environment is generally nonhomogeneous and cannot contain all reference cells Independent and Identically Distributed (IID), a reference window may contain clutter-edges and multiple targets, which are the main causes of the heterogeneity of the environment [4–8].

Perturbation is one of the undesirable phenomena that affect the quality of detection. This perturbation is represented as a set of complex normal random vectors plus deterministic interference in a specified subspace. They assumed that they had access to a noise-only data set with the same statistical characterization of the noise in the cells tested. They used either the simple Generalized Likelihood Ratio Test (GLRT) or the two-stage GLRT-based design stage [9].

The challenge of adaptive recognition of multidimensional/multichannel signals in homogeneous Gaussian perturbations with unknown covariance matrices and organized deterministic interference is addressed in [10]. According to [10], all detectors are Maximal Invariant Statistics (MIS) functions, which demonstrates their CFAR characteristic.

The effected work in [11] concentrates on the classic problem of testing samples generated from independent Bernoulli probability mass functions while the alternative hypothesis' success probability is unknown. With regard to same success probabilities or different success probabilities for the observed samples, both One-Sided and Two-Sided tests are evaluated. The existence of the Uniformly Most Powerful (UMP) detector after reduction by invariance is studied when the Likelihood Ratio Test (LRT) is not UMP.

In these cases, the detection system suffers from numerous false alarms and masking of real targets [12].

To perform a processing CFAR and for detecting the radar signal, an adaptive threshold must be utilized. This detection threshold is calculated using the power of the adjacent distance cells, located on both sides of the cell under test (CUT) [13, 14], which are used to measure the clutter's power level and will be compared with that of the CUT to give a binary decision H_0 or H_1. The threshold calculation of previous classical CFAR detectors does not have any priori knowledge about the clutter environment, that is to say, each CFAR detector is ideal for a particular environment and not for all [2].

However, the reality shows that the condition of Gaussian and homogeneity of the environment is not always verified [15–17]. This is interpreted by the dynamic change of the environment of the radar generated by the presence of the different types of clutter (land, sand, sea, forest, etc.) [18] which causes a degradation in the performance of CFAR detectors resulting in a loss of detection and generation of supplementary false alarms. One possible solution to overcome these limitations is the use of the priori knowledge about the environment to remove the non-homogeneity of the environment and to make the radar a smart device [12].

Our contribution in this work concerns a part of the radar signal processing to design a robust and dynamic KB. This KB will provide a data selector to select among the cells of the sliding window, which are similar to the CUT. The detection system is then able to correctly use the CFAR detectors in their favorable conditions thanks to this priori knowledge of the environment, thus enhance the detection performance and minimize additional false alarms. The Weibull distribution assumed in this study is a non-Gaussian distribution that is frequently utilized in clutter modeling, since it is quite good at fitting empirical radar data and can represent different types of clutter [19].

This article is organised as follows. In Section 2, we present the sources of knowledge about the environment, KBS. Sections 3 and 4 give a detailed study for general and special Weibull parameters in homogeneous and nonhomogeneous situations. Section 5 will be reserved for the implementation and discussion of results. Finally, the conclusion and perspectives are given in Section 6.

NOTATION PARAGRAPH

H_1 in the INTRODUCTION means a presence of the target hypothesis, while H_0 represents the absence of the target hypothesis. In Section 2.2, M-N denotes a sliding clutter edge locator with an M out of N detection. In Section 2.2.1, X, $[\cdot]^T$, and N represent respectively a vector of reference data, transpose, and size of reference window; $\widehat{k}$ refers to the estimated position of the clutter edge. In Section 2.3.2, $P_n(i,j)$ and w denote the terminal value of the cell's attribute (i,j) and the weighting factor. In Section 2.4, S_{cut} and D_{cut} are SEKB and DEKB of the cell under test, while S_i and D_i are the ones provided by the GIS, and B and C represent respectively the scale and shape parameters. In

Section 3.1.1, t denotes a statistical test, while W represents a data set by a Gumbel distribution; T and $T_{\text{Log-t}}$ are the detection threshold and scaling factor. In Section 4, λ and σ denote inverse scale and scale parameters. Finally, in Section 4.2.1, $D(i)$ and Ω stand for a homogeneity indicator and the set of K_s smallest indices, respectively.

2. SOURCES OF KBS

The radar detection capability is always linked to the knowledge of the radar environment. As long as this knowledge is great, the radar detection capability is improved. This knowledge makes it possible to calculate the detection threshold using the reference cells most similar to the CUT.

2.1. Geographic Information System

GIS has evolved into a sophisticated and extensively used technology, with a growing role in GPS functionality and route optimization. GIS is an integrated system for processing and interpreting geospatial data that uses these homogeneous elements to model geographic data. In radar detection with GIS, we can utilize a data selector to select cells that have a GIS index similar to CUT to determine the CFAR detector's threshold [20].

2.2. Homogeneous Reference Cells Selector

The M-N clutter edge detector has been proposed to detect a possible clutter edge in the cells of the reference window [21], but this technique has limitations in the case of a radar environment containing more than one clutter edge, and as an improvement of this M-N clutter edge detector, the researchers proposed the Homogeneous Reference Cells Selector (HRCS).

This selector combines an M-N clutter edge detector with a terrain classifier in a cascade [22].

2.2.1. M-N Clutter Edge Detector

A sliding window of length N slides over distance cells from left to right. With each slide, to find the position of a likely clutter edge, we employ a clutter edge locator. The following is an illustration of the clutter edge locator's process [22]:

- Begin with the reference data:
$$X = [X_1, \ldots, X_N]^T \text{ of length } N \text{ and } \zeta = 2\ln(N).$$
- For $k = 0, 2, \ldots, N-1$, calculate:
$$f(k) = \begin{cases} N\ln(\text{Std}(X)) - \zeta & k = 0 \\ (N-k)\ln(\text{Std}(z)) + k\ln((y)) & 1 \le k \le N-1 \end{cases}$$
where $y = [y_1, \ldots, y_k]^T$, $z = [z_{k+1}, \ldots, z_N]^T$, and $\text{Std}(\cdot)$ represents the value of the mean square.
- The position of the clutter edge will be at $\widehat{k} = \arg_k \min f(k)$.

This means that the estimated position $\widehat{k}$ is the value of k which corresponds to the minimum value of $f(k)$. If $\widehat{k} = 0$, there is no clutter edge.

2.2.2. Terrain Classifier

With the clutter edge detected, the classifier for terrain is used to obtain the IID reference cells.

For this, we consider the following basic principles:

- Distance cells in the reference window with an IID identical to the CUT are included even if they are far from it.
- Distance cells with a different IID to the CUT are not included in the reference window even if they are just next to it. The scale and shape parameters of the regions between two neighboring clutter edges are estimated; then we classify these parameters, and the terrains with the same IID are selected.

2.3. Dynamic Update of Environmental KB

The main stages of Dynamic update of Environmental KB (DEKB) are [23–25]:

2.3.1. Static Environmental Knowledge Base

Unlike the traditional earth clutter map, which only offers absolute values of the reflection coefficient for a radar resolution cell's spatial coordinates [26, 27], the Static Environmental Knowledge Base (SEKB) map contains a lot of priori knowledge additionally to the reflection coefficient.

2.3.2. Dynamic Updating

The radar and other cooperating sensors interact with the environment and obtain up-to-date information. For the nth update, the attribute value becomes as mentioned in Equation (1):

$$P_n(i,j) = (1-w) * P_{n-1}(i,j) + w * P_n(i,j) \tag{1}$$

where

$P_n(i,j)$: the terminal value of the cell's attribute (i,j).

w: weighting factor between 0 and 1.

As w increases, the last attribute value depends on the new data other than the previous one.

2.4. Principle of the Proposed CEKB

The proposed structure of the CEKB mentioned in Fig. 1 contains two elements:

The first is to create the SEKB by data extraction from a GIS [28].

The surveillance area is divided into small grids (x_i, y_j). The entire area is handled as a matrix, whose each cell has an attribute value, and the resulting attribute values are determined from the corresponding attribute values [29].

Because the SEKB could not suit the real radar operating environment for a variety of reasons, extra data are required to dynamically match the radar operating environment.

The second part is the usage of selector for homogeneous reference cells [22] to create and update the DEKB using radar returns in real time to keep the KB matching the detecting environment.

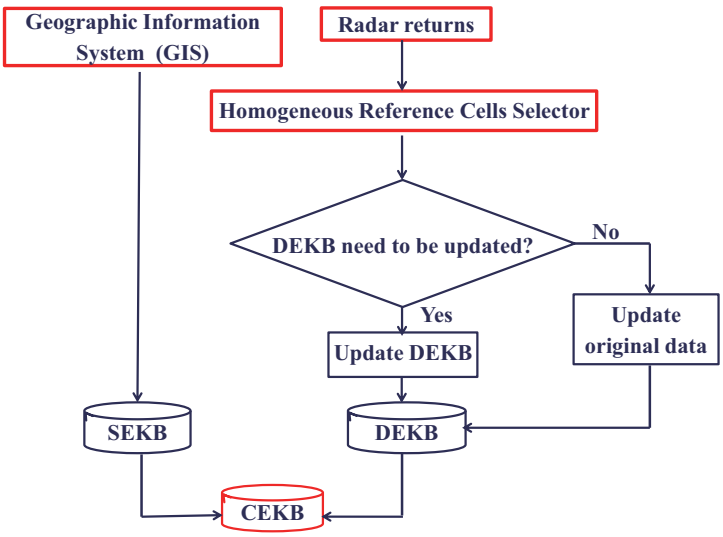

Figure 1. Block diagram of the proposed CEKB.

The suggested CEKB's data selector idea is to receive data for each cell X_i, a CEKB $C_i = (S_i, D_i)$, where S_i is the SEKB provided by GIS, and D_i is the DEKB generated after applying the M-N clutter edge detector and classifier of terrain.

For each CUT, we use a sliding window of K cells, with $K = 2 * N$, where N represents the number of used reference cells.

For $i \in \{1, \ldots, K\}$, we denote:

$$\begin{aligned} dS_i &= abs\left(S_{cut} - S_i\right); \\ dD_i &= abs\left(D_{cut} - D_i\right); \\ d_i &= dS_i + dD_i; \end{aligned}$$

with S_{cut} and D_{cut} being SEKB and DEKB of the CUT, respectively, and after that we select N cells with the lowest values of d_i and in the nearest region of the CUT.

3. GENERAL WEIBULL PARAMETERS

3.1. Homogeneous Environment

The Probability Density Function (PDF) of Weibull is a two-parameter distribution, a special case of which is the Rayleigh distribution and the Exponential is the other. This study assumes that the background, supposed Weibull, does not have any prior knowledge about the environment, and its PDF can be described by Equation (2):

$$f(x) = \frac{C}{B}\left(\frac{x}{B}\right)^{C-1} \exp\left[-\left(\frac{x}{B}\right)^{C}\right] \tag{2}$$

where B represents the scale parameter, and C represents the shape parameter.

3.1.1. Log-t-CFAR

The Log-t-CFAR was proposed by Goldstein in 1973 for Log-normal and Weibull clutter. This detector is the best for Log-normal clutter and works well for homogeneous Weibull clutter [30].

When the clutter is Weibull, the distribution of x_i follows the form given by Equation (2), with $x > 0$, so $y_i = \ln x_i$ follows the distribution of Gumbel [21]:

$$f(y, a, b) = \frac{1}{a} \cdot \exp\left[\frac{y-b}{a} - \exp\left(\frac{y-b}{a}\right)\right] \tag{3}$$

Considering these transformations: $a = 1/C$ and $b = \ln B$ that are Gumbel's parameters, we can obtain the Gumbel's distribution referred by Equation (4):

$$\ln(f(y, a, b)) = -\ln a + \frac{y-b}{a} - e^{\frac{y-b}{a}} \tag{4}$$

The proposed statistical test is given for the distribution of observations y_i, $i \in [0, \ldots, N]$ in the presence of the Weibull clutter. The CUT is y_0, and parameter t is given by Equation (5) [30]:

$$t = \frac{y_0 - \dfrac{1}{N} \cdot \displaystyle\sum_{i=1}^{N} y_i}{\sqrt{\dfrac{1}{N}\displaystyle\sum_{i=1}^{N}\left(y_i - \dfrac{1}{N}\displaystyle\sum_{k=1}^{N} y_k\right)^2}} = \frac{y_0 - \hat{\mu}_y}{\hat{\sigma}_y} \tag{5}$$

where we see that all N cells are included in the test.

Note that when the clutter alone is present, the numerator of "t" implies subtracting the Maximum Likelihood (ML) estimate from the mean of the CUT, and the denominator of "t" normalizes the variable by dividing the ML estimate of the standard deviation of the reference cells.

We consider the following transformation [21]:

$$G_{\alpha,\beta} = \left\{\alpha * y_i + \beta, \alpha \text{ and } \beta \in R^+ \text{ and } y_i = [y_1, y_2, \ldots, y_N] \in W\right\} \tag{6}$$

where α and β represent the scale and shape parameters, respectively. Under the assumption H_0, the data set is IID by a Gumbel distribution. It is proved that the transformed data by the $G_{\alpha,\beta}$ group also have a Gumbel distribution.

Furthermore, the statistics of the transformed data $G_{\alpha,\beta}(W)$ are mentioned in Equations (7) and (8):

$$\text{Mean}\left(G_{\alpha,\beta}(W)\right) = \alpha * \text{mean}(W) + \beta \tag{7}$$

$$\text{Std}\left(G_{\alpha,\beta}(W)\right) = \alpha * \text{Std}(W) \tag{8}$$

The detection threshold for Log-t-CFAR detector is given by Equation (9):

$$T = \mathbf{T}_{\text{Log-t}} * \widetilde{\mathbf{Std}} + \widetilde{\mathbf{Mean}} \tag{9}$$

where $T_{\text{Log-t}}$ represents scaling factor.

3.1.2. ML-CFAR

In homogeneous Weibull case, the Maximum Likelihood-CFAR (ML-CFAR) detector outperforms the Log-t-CFAR detector. Computationally, this detector is expensive, and its output is more homogeneous-sensitive [31]. Maximum Likelihood Estimators for the scale parameter B and shape parameter C are obtained from the M samples:

$$x = (X_1, X_2, \ldots, X_M)^T.$$

The scaling factor B depends on the number of reference samples M and P_{fa}.

To determine the estimated value of $C(\hat{C})$, it is sufficient to solve Equation (10):

$$\frac{\sum_{j=1}^{M} x_j^{\hat{c}} \ln x_j}{\sum_{j=1}^{M} x_j^{\hat{c}}} - \frac{1}{M} \cdot \sum_{j=1}^{M} \ln x_j = \frac{1}{\hat{c}} \tag{10}$$

Using the value of C, we can determine B from Equation (11):

$$\hat{B} = \left(\frac{1}{M} \cdot \sum_{j=1}^{M} x_j^c\right)^{\frac{1}{\hat{c}}} \tag{11}$$

When the scale parameter B and shape parameter C are unknown, they must be estimated at the same time using the reference samples. The threshold will be determined by the following expression, which is dependent on the estimation of B and C:

$$T = \hat{B} * \alpha^{\frac{1}{\hat{C}}} \tag{12}$$

where $\alpha = \ln(1/P_{fa})$ represents the scaling factor.

3.1.3. Simulation Results

The simulations in Fig. 2 and Fig. 3 have parameters: probability of false alarm P_{fa}, number of samples N_s, size of reference window N, and their values are mentioned in Table 1.

Fig. 2 represents the detection thresholds of the ML-CFAR and Log-t-CFAR detectors for a homogeneous Weibull clutter with the presence of the three separate targets for a scale parameter B and shape parameter C indicated also in Table 1.

We find from Fig. 2 that these detectors are the most suitable for a homogeneous Weibull clutter because they present the minimum of false alarms and detect all existing targets.

Table 1. The parameters of Fig. 2 and Fig. 3.

P_{fa}	N_s	N	(B, C)	(B_1, C_1)	(B_2, C_2)
$(10)^{-5}$	100	16	$(1, 3)$	$(1, 4)$	$(4, 1)$

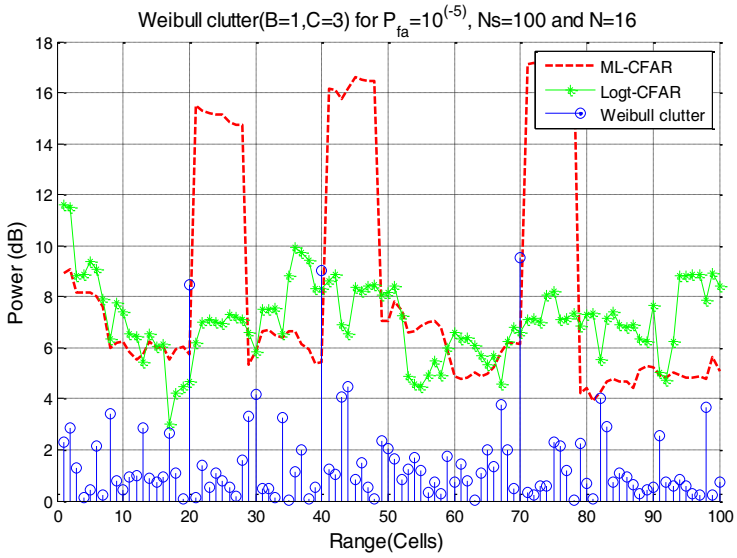

Figure 2. ML and Log-t-CFAR in homogeneous Weibull clutter.

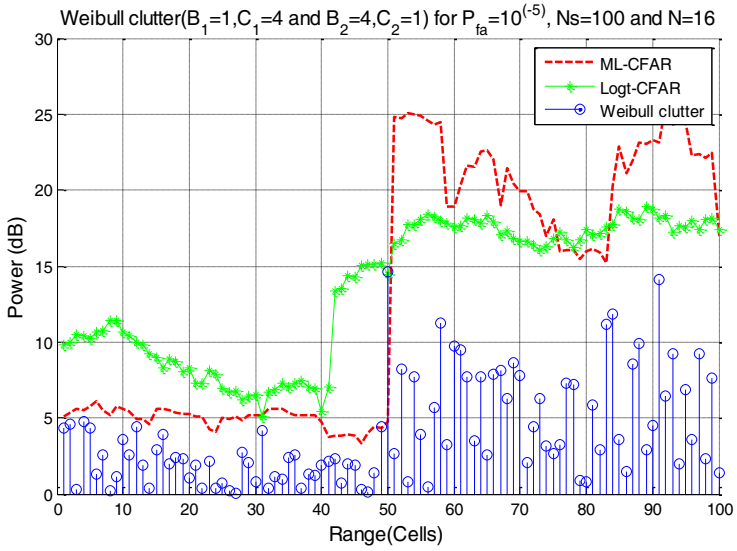

Figure 3. Degradation of ML and Log-t-CFAR in nonhomogeneous Weibull clutter.

The simulation result in Fig. 3 represents a nonhomogeneous Weibull environment caused by the presence of two regions that have different scale and shape parameters. This implies the presence of a clutter edge between these two regions (at range cell = 50). It will cause an undesirable detection of this clutter edge which results in the generation of additional false alarms and involves the degradation and performances limitation of the ML-CFAR and Log-t-CFAR detectors in a nonhomogeneous Weibull environment.

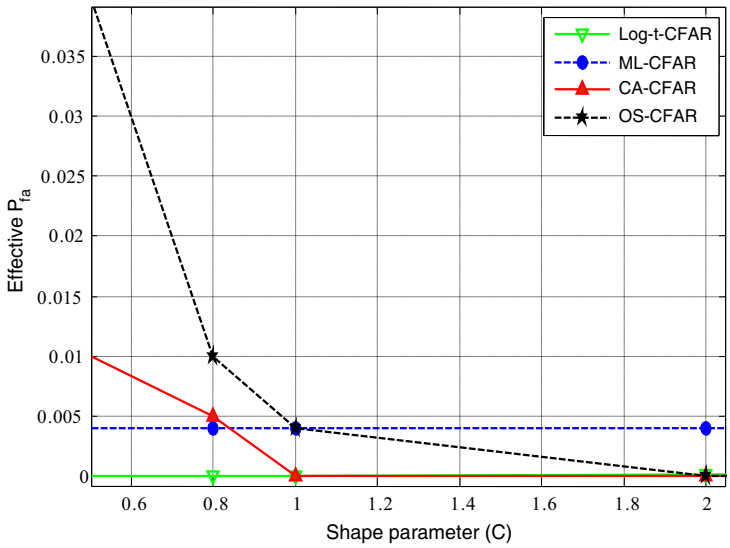

Figure 4. False alarm regulation.

A comparative simulation among the ML, Log-t, CA (Cell Averaging), and OS (Ordered Statistic)-CFAR detectors in terms of preservation of the desired P_{fa} gives the result in Fig. 4.

From Fig. 4, the Logt-CFAR carefully preserves the desired P_{fa}. The ML-CFAR also preserves the desired P_{fa} but at higher value than the desired one. The CA-CFAR detector has 02 steps; the first one for shape parameter $C < 1$ where the effective P_{fa} decreases in an almost linear way from a value of 10^{-2} for C tends to 0, to a value of 10^{-3} when C tends to 1, and in the second one, it will be constant at the desired value when $C > 1$. The OS-CFAR detector no longer preserves the desired P_{fa}.

3.2. Nonhomogeneous Environment

Non-homogeneity of the clutter appears as one or more clutter edges along the sliding reference window over the radar coverage area. We will propose KBS-CFAR architectures by considering CEKB as a source of knowledge to remove this non-homogeneity.

3.2.1. KBS-Log-t-CFAR Detector

The principle of the KBS-Log-t-CFAR detector consists of integrating the CEKB into the Log-t-CFAR detector; then a data selector will determine areas of homogeneity in the reference window, and a Log-t-CFAR detector is applied to the regions similar to the CUT.

3.2.2. KBS-ML-CFAR Detector

The principle of the KBS-ML-CFAR detector is similar to KBS-Log-t-CFAR, except that this KBS-ML-CFAR will apply the algorithm of the ML-CFAR detector to samples from the reference window which are identical to the CUT designated by the CEKB.

The block diagram of the proposed KBS-CFAR architectures is illustrated in Fig. 5.

3.2.3. Simulation Results

The simulation in Fig. 6 has parameters: P_{fa}, N_s, N, and their values are given in Table 2.

This simulation shows a zone that follows Weibull distribution with different parameters (B_1, C_1), (B_2, C_2), and (B_3, C_3) mentioned in Table 2. It is the equivalent of a nonhomogeneous Weibull environment associated with the presence of the two clutter edges.

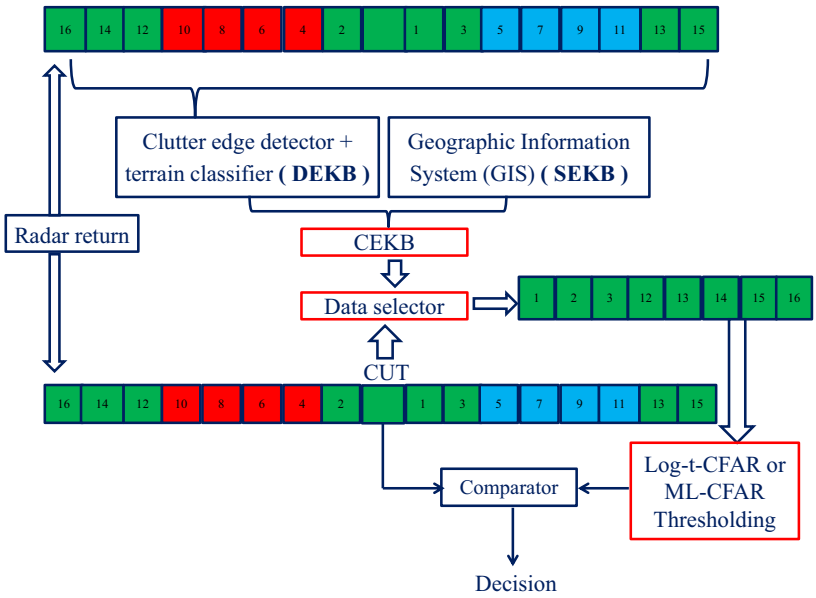

Figure 5. Architecture of KBS-CFAR detector.

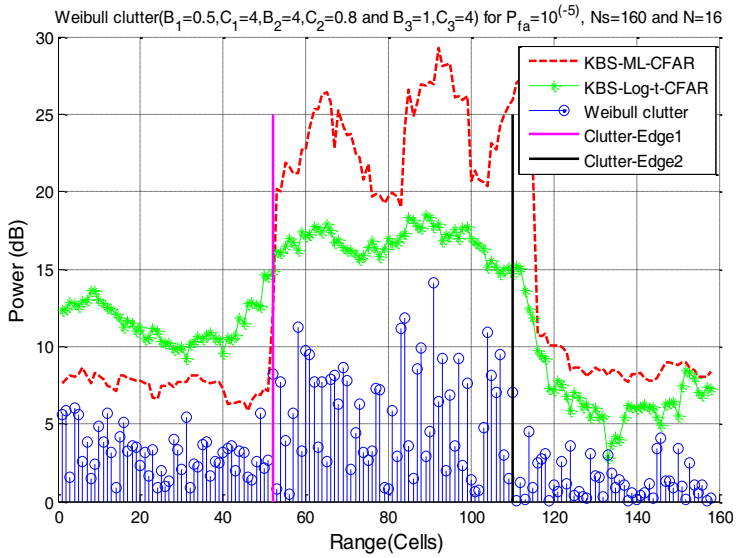

Figure 6. Performances of KBS-Log-t-CFAR and KBS-ML-CFAR in nonhomogeneous Weibull clutter.

Table 2. The parameters of Fig. 6.

P_{fa}	N_s	N	(B_1, C_1)	(B_2, C_2)	(B_3, C_3)
$(10)^{-5}$	160	16	$(0.5, 4)$	$(4, 0.8)$	$(1, 4)$

From Fig. 6, it is clear that the CEKB detects the two clutter edges. The algorithm of the detectors ML-CFAR and Log-t-CFAR will be applied to the cells that make up the reference window and share the same IID as the CUT. It results in a minimization of false alarms around the clutter edges and makes the operation of the two detectors mentioned above in a nonhomogeneous environment similar to the ML-CFAR and Log-t-CFAR detectors in a homogeneous Weibull clutter.

To show the false alarm probability regulation of the proposed KBS-Log-t-CFAR based on CEKB, we study its effective P_{fa} compared with that of Modified Log-t-CFAR based on HRCS in [22].

Fig. 7 demonstrates that even in the presence of clutter edges, the Modified Log-t CFARD maintains the desired P_{fa} for a variety of shape parameter values, except for clutter edges with weak Clutter to Clutter Ratio, CCR (cell 151) when the effective P_{fa} attempts $2.6 * \text{desired}\, P_{fa}$.

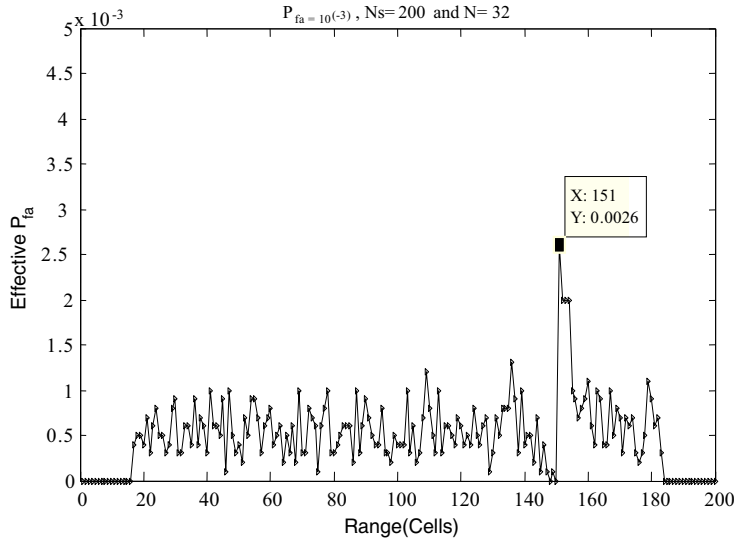

Figure 7. Effective P_{fa} for Modified Log-t-CFAR based on HRCS.

Fig. 8 shows that the proposed KBS-Log-t-CFAR detector based on CEKB outperforms the Modified Log-t-CFAR based on HRCS to maintain the desired P_{fa} for various shape parameter values and in the presence of many clutter edges. Table 3 presents the parameters used for Fig. 7 and Fig. 8.

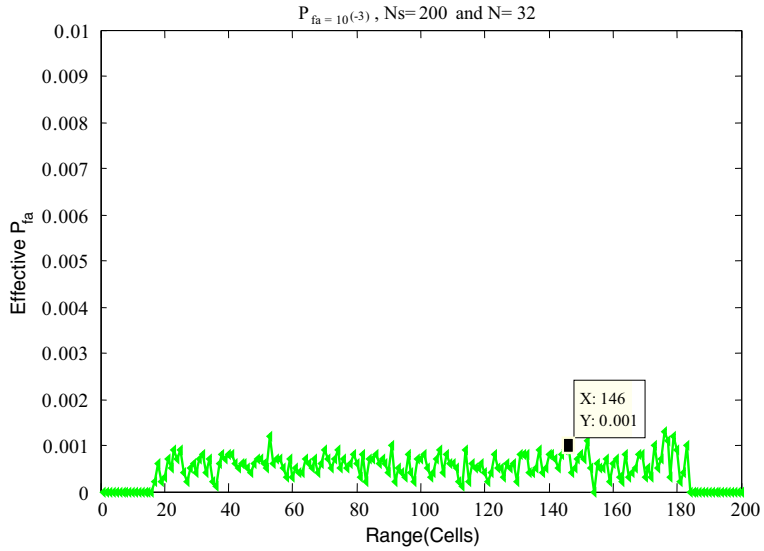

Figure 8. Effective P_{fa} for the proposed KBS-Log-t-CFAR based on CEKB.

4. SPECIAL WEIBULL PARAMETERS

We consider Equation (2) that describes the Weibull PDF:

Table 3. The parameters of Fig. 7 and Fig. 8.

P_{fa}	N_s	N
$(10)^{-3}$	200	32

We replace the shape parameter $C = 1$ in Equation (2), and it becomes Equation (13):

$$f(x) = \frac{1}{B} * \exp\left[-\left(\frac{x}{B}\right)\right] \tag{13}$$

We suppose $\lambda = \frac{1}{B}$, and Equation (13) becomes Equation (14):

$$f(x) = \lambda * \exp[-\lambda x] \tag{14}$$

which is the PDF of the exponential distribution, and its rate or inverse scale is $\lambda = \frac{1}{B}$.

We replace the shape parameter $C = 2$ in Equation (2) and find Equation (15):

$$f(x) = \frac{2}{B} \cdot \left(\frac{x}{B}\right) \cdot \exp\left[-\left(\frac{x}{B}\right)^2\right] \tag{15}$$

We suppose $\sigma = \frac{B}{\sqrt{2}}$, and Equation (15) becomes Equation (16):

$$f(x) = \frac{x}{\sigma^2} \exp\left[-\left(\frac{x}{\sqrt{2} \cdot \sigma}\right)^2\right] \tag{16}$$

which is the Rayleigh PDF, and his scale parameter is: $\sigma = \frac{B}{\sqrt{2}}$.

So, these two derivatives from Weibull PDF are the subject of the following study.

4.1. Homogeneous Environment

We suppose in this part a situation where no any previous knowledge of the environment is provided. According to Fig. 9, we summarize the characteristics of each detector as follows:

The CA-CFAR detector and its derivatives (GO (Greatest Of) and SO (Smallest Of)) are designed for their preferred environments.

The CA-CFAR [1] is best suited to a homogeneous environment.

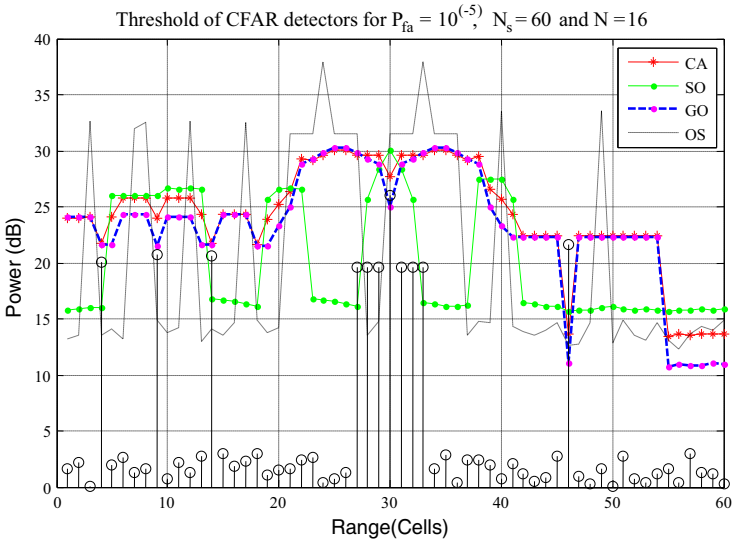

Figure 9. Performances of classical detectors.

Its derivative SO-CFAR [32] concerns interfering targets present in one half sliding window. OS-CFAR [33] prefers the environment with interfering targets, and GO-CFAR [34] is efficient in the case of clutter edge presence.

4.2. Nonhomogeneous Environment

In practice, the environment's dynamic change degrades the performances of those conventional detectors which are originally specified for a given type of environment. To remove this non-homogeneity, we need previous information about the environment of the radar [12].

This knowledge can facilitate the selection of training samples that participate in the estimation of the detection threshold. We will propose several techniques for solving the problem of detection loss and additional false alarms generated by nonhomogeneous environment presence. We will present a study of nonhomogeneous and interfering Rayleigh and Exponential clutter considering the GIS as a KB.

4.2.1. Without Interference Case

KBS-Static and KBS-Dynamic are two detectors that use the KBS in determining the detection threshold [35].

- KBS-Static-CFAR:

The relevant properties to the CUT and K reference cells can be determined using the GIS. $D(i)$ is a homogeneity indicator that is also evaluated as follows [23, 35]:

$$D(i) = \begin{cases} 0 & si \quad x_i \neq x_{Cut} \\ 1 & si \quad x_i = x_{Cut} \end{cases} \tag{17}$$

The following are the indices of the chosen data collected from the set Ω:

- If $\sum_{i=1}^{k} D(i) > K_s$ and if $D(i) = 1$ and K_s is a constant, then Ω refers to the set of K_s smallest indices.

It is the same as selecting the homogeneous cells K_s in the closest space to the CUT as formation data.

- If $\sum_{i=1}^{k} D(i) < K_s$ and Ω is composed of cell indices that are homogeneous and $Ks - \sum_{i=1}^{k} D(i)$ is made up of nonhomogeneous cell indices closest to the CUT.

A CA-CFAR detector is utilized to take the final decision on the presence of the target after the cells selection process.

- KBS-Dynamic-CFAR:

The key distinction between KBS-Static-CFAR and KBS-Dynamic-CFAR is that the first one needs a fixed number of K_s cells, while the second selects them dynamically as an interval $[K_{\min}, K_{\max}]$.

4.2.2. Simple Interference Case

- KBS-OS-CFAR:

The principle of the KBS-OS-CFAR detector is to select among the reference window's cells which have the similar GIS, to order them and then to take the kth sample as the detection threshold, such as $K = 3 * N/4$, where N represents the cells number similar to the CUT.

- KBS-ALC-CFAR:

The KBS-ALC-CFAR (KBS-Adaptive Linear Combined) detector mixes the performances of the KBS-Dynamic with the performances of KBS-OS-CFAR. To take advantage of the KBS-ALC detector, we apply its algorithm to the selected samples for threshold estimation using Equation (18) [36, 37]:

$$\text{Threshold}_{\text{KBS-ALC}} = \alpha * \text{Threshold}_{\text{KBS-Dynamic}} + (1 - \alpha) * \text{Threshold}_{\text{KBS-OS}} \tag{18}$$

$\text{Threshold}_{\text{KBS-Dynamic}}$: average of samples designed by KBS-Dynamic-CFAR process.

$\text{Threshold}_{\text{KBS-OS}}$: choosing of the Kth sample ($K = 3 * N/4$) designed by N sorted samples of KBS-Dynamic-CFAR process.

α represents the degree of homogeneity.

For $\alpha = 1$;

$\text{Threshold}_{\text{KBS-ALC}} = \text{Threshold}_{\text{KBS-Dynamic}}$;

For $\alpha = 0$;

$\text{Threshold}_{\text{KBS-ALC}} = \text{Threshold}_{\text{KBS-OS}}$;

For $0 < \alpha < 1$;

$\text{Threshold}_{\text{KBS-ALC}}$ is given by the formula of Equation (18).

4.2.3. Severe Interference Case

- Proposal for a new technique KBS-FAOSOS-CFAR:

For a severe interference case, we propose a new approach to deal with both the non-homogeneity interpreted by the existence of different GIS and the severe interference in the sliding window [6].

The principle of KBS-FAOSOS-CFAR detector relies on the application of the Information Theoretic Criterion (ITC) concept. The proposed design aims to enhance the effectiveness of the KBS-OS-CFAR detector in cases of significant interference. The interfering targets number is determined by minimizing the ITC [38].

Fig. 10 shows the architecture of the KBS-FAOSOS-CFAR detector.

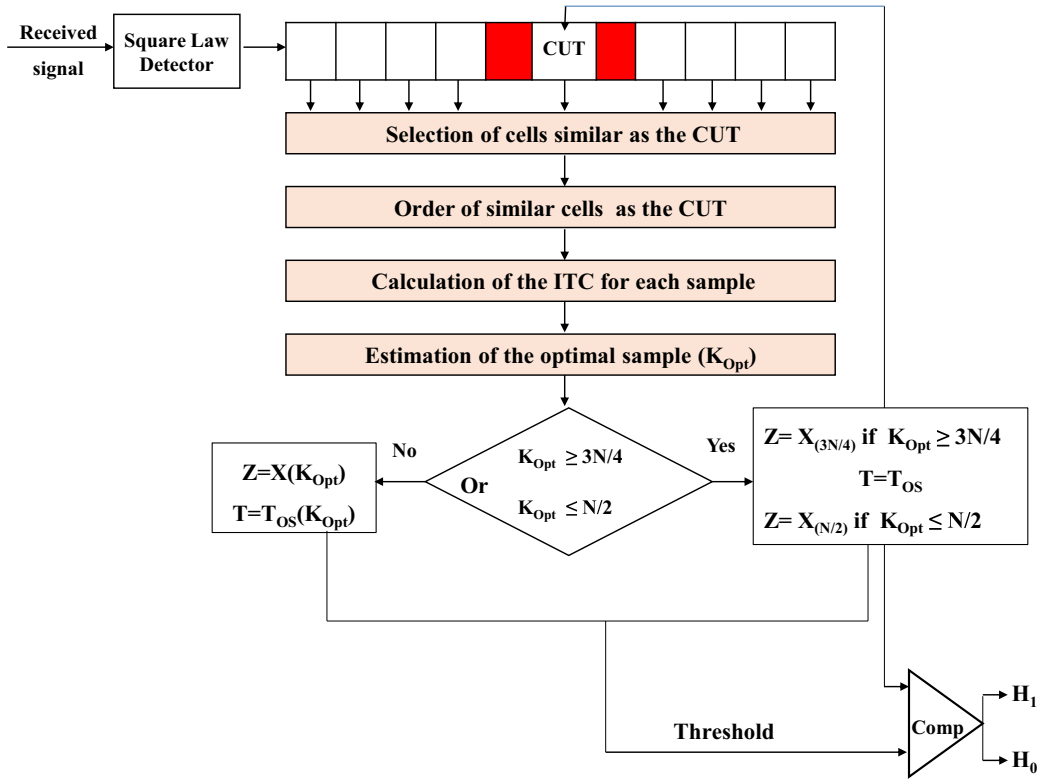

Figure 10. Architecture of KBS-FAOSOS-CFAR.

The radar echo received for this technique passes through the square law detector; then the radar outputs X_i, $(i = 1, ...N)$ are saved in a register of size $N+1$. The cell located in the center is the CUT, where it contains the signal that we want to know its content H_0 or H_1. The N cells of the sliding window are used to calculate the CFAR threshold.

The ITC is defined as follows [39–41]:

$$\mathrm{AIC}(k) = -2(N-k)N \ln\left(\frac{G(\lambda_{k+1},...,\lambda_N)}{A(\lambda_{k+1},...,\lambda_N)}\right) + 2k(2N-k) \tag{19}$$

for the Akaike Information Criterion (AIC).

$$\mathrm{MDL}(k) = -(N-k)N \ln\left(\frac{G(\lambda_{k+1},...,\lambda_N)}{A(\lambda_{k+1},...,\lambda_N)}\right) + \frac{k(2N-k)\ln N}{2} \tag{20}$$

for the Minimum Description Length, MDL, Criterion, where $\lambda_1 > \lambda_2 > \cdots > \lambda_N$ indicates the samples of the sliding window in our situation; N represents the number of samples; G and A are the geometric and arithmetic averages of their arguments, respectively.

The order $k \in \{0, 1, \ldots, N-1\}$ of the KBS-OS-CFAR detector is considered for which AIC(k) or MDL(k) are minimized which allows for the detection of interfering target groups to be done automatically [38].

4.2.4. Simulation Results

The simulations represented by Fig. 11, Fig. 12, and Fig. 13 have parameters: $P_{fa} = 10^{(-4)}$, $Ns = 60$, and $N = 16$.

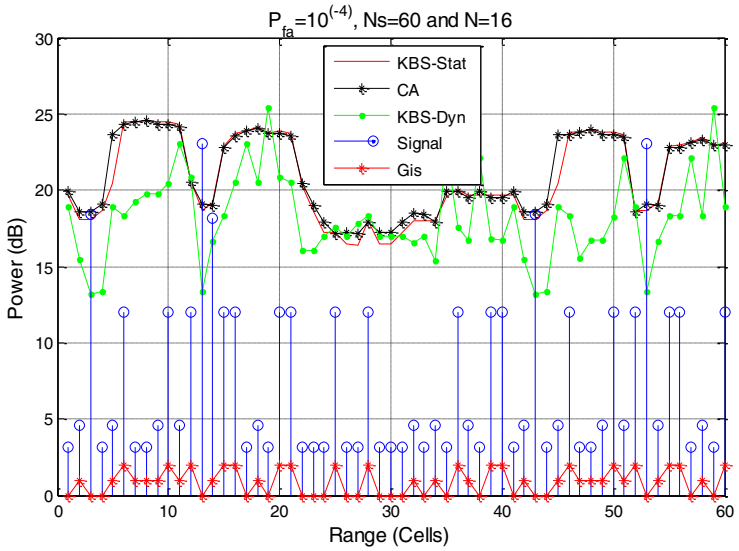

Figure 11. Performances of KBS-Dynamic, KBS-Static and CA-CFAR detectors basing on GIS.

From Fig. 11, we can see that the KBS-Dynamic detector is most suitable for a situation of simple interference, such as this interference occurring in cells that have a different GIS since it estimates its threshold using reference cells that have the same GIS as the CUT.

This is the case of the interfering targets located at positions 13 and 14 that have respectively the GIS 0 and 1.

This choice is made dynamically, i.e., if this number of cells is not sufficient for the estimation of the threshold, it will take other cells which have a value of GIS close to the CUT. This dynamic choice of cells is found neither in the KBS-Static detector which has a fixed number of these cells nor in the classic detector CA-CFAR which has not any prior information on the environment and makes only the averaging.

The simulation in Fig. 12 presents two possible cases:

The first case concerns interfering targets located at reference cells: 47, 48, and 50 which have the same GIS = 1.

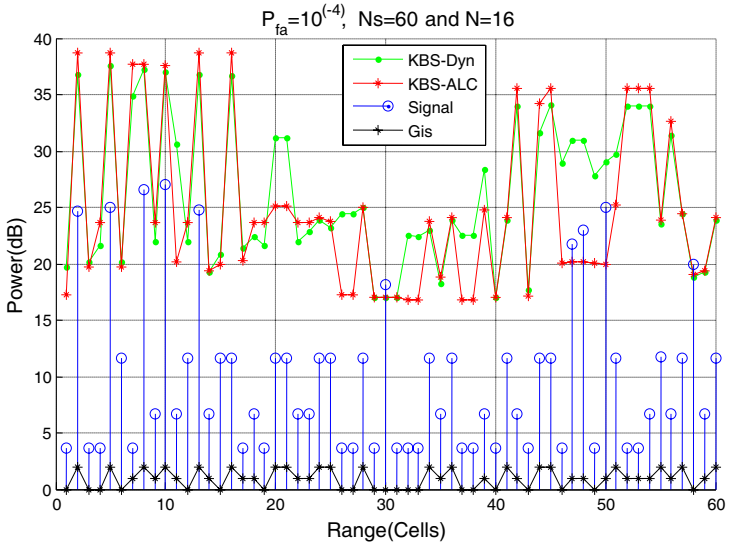

Figure 12. Performance of KBS-ALC-CFAR detector.

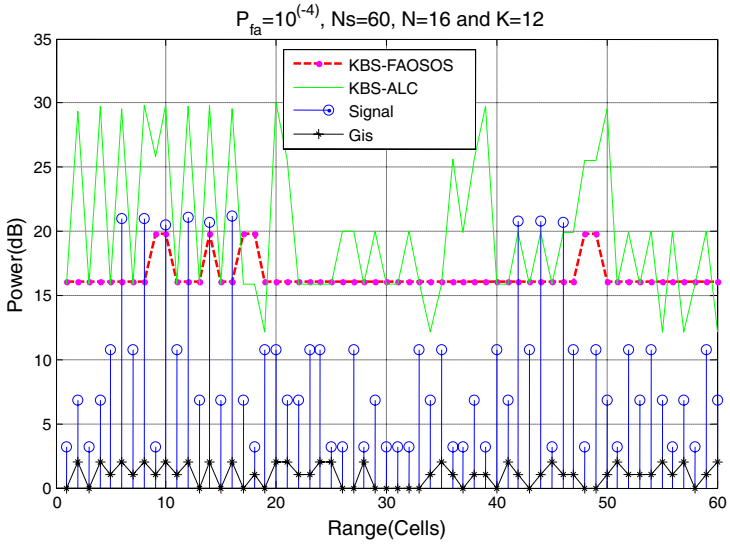

Figure 13. Performance of KBS-FAOSOS-CFAR detector.

When the CUT is located at a cell that has this same GIS = 1, it will take all these interfering targets to calculate the detection threshold. The threshold resulting from the KBS-Dynamic detector will be increased which causes the masking of these 3 interfering targets, and the KBS-Dynamic detector will be not more powerful.

The KBS-ALC detector becomes efficient in this case (interfering target with same GIS as the CUT) because it balances its functioning towards the KBS-OS detector. The KBS-ALC detector remains efficient while the number of interference targets is lower than $N-K$ (in our case: number of interference $= 3 < N - K = 16 - 12 = 4$).

The second case concerns a group of 5 interfering targets located at positions: 2, 5, 8, 10, and 13 with the same GIS = 2. This case makes the KBS-ALC detector no longer performing, because the number of interfering targets is greater than $N-K$ (Number of interfering targets $= 5 > N-K = 16-12 = 4$), and this is the case of severe interference.

According to the simulation in Fig. 13, there are two possible situations:

One case concerns 3 interfering targets located at samples: 42, 44, and 46 which have the same GIS = 1. These 3 interfering targets are detected by the two detectors KBS-ALC and KBS-FAOSOS-CFAR (Simple interference case).

Another case concerns a set of 6 interfering targets located at cells: 6, 8, 10, 12, 14, and 16 which have the same GIS = 2.

We note that the KBS-ALC detector loses its performance completely in this case. On the other hand, the KBS-FAOSOS-CFAR detects all these targets thanks to its algorithm which enables it to identify and detect the group of interfering targets that have the same GIS as the CUT.

5. IMPLEMENTATION RESULTS

We present the implementation results of some CFAR detectors using ADSP processing board [42] that has a 600 MHz core clock speed, followed by a discussion of the obtained results and the execution time.

We consider signals received from a radar that has the following parameters:

With a PRF of 1200 HZ, PRT = 0.833 ms, angular resolution = 1.4°, pulse width $\tau = 1\,\mu$s, and antenna rotation speed = 12 rpm.

The implementation results are obtained for $P_{fa} = 10^{(-5)}$, size of reference window $N = 16$, and a number of samples $N_s = 63$ cells.

3 phases of received signals are present; the first one concerns an isolated target; the second one contains interfering targets 2 and 3 that have different GIS; and the third one represents a group of interfering targets 4, 5, and 6 that share the same GIS.

5.1. Implementation Results of Classical Detectors

From Fig. 14, we can see that the implementation of the CA-CFAR detector has proven its performance in detecting isolated targets embedded in a homogeneous environment and that this detector is no longer efficient for interfering targets case where the OS-CFAR detector mentioned by Fig. 15 is the most efficient.

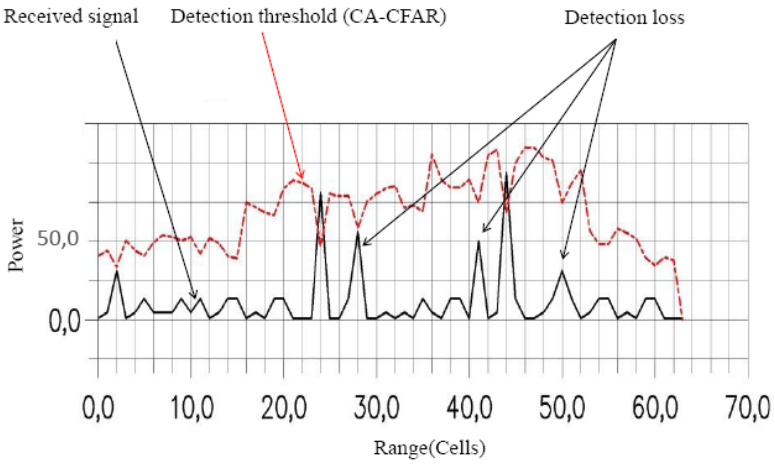

Figure 14. Implementation of CA-CFAR.

5.2. Implementation Results of KBS-CFAR Detectors

Fig. 16 shows the implementation result of the KBS-Dynamic-CFAR detector for a size of reference window $N = 16$, $K_{\max} = 14$, $K_{\min} = 8$, $P_{fa} = 10^{(-5)}$, and for 63 cells.

The implementation result shows the effect of the prior knowledge exploitation on the environment in the improvement of the target detection. The KBS-Dynamic detector detects the first isolated target and also detects the two targets with different GIS, but it misses the last target among 3 interfering targets that have the same GIS.

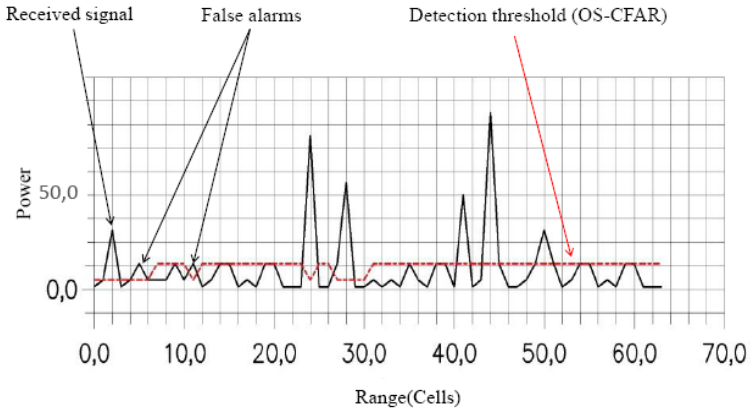

Figure 15. Implementation of OS-CFAR.

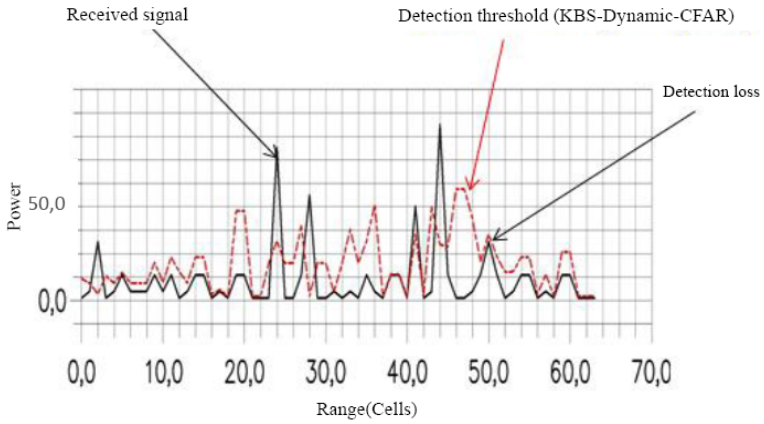

Figure 16. Implementation of KBS-Dynamic-CFAR.

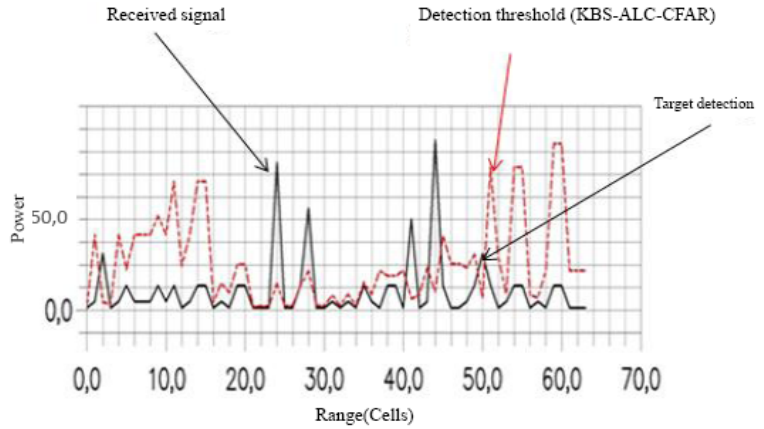

Figure 17. Implementation of KBS-ALC-CFAR.

From the implementation result of the KBS-ALC-CFAR detector mentioned in Fig. 17, we can confirm the performance of the KBS-ALC-CFAR detector which exploits both the performance of the KBS-Dynamic detector in a homogeneous environment and the performance of the KBS-OS-CFAR detector in an interfering target environment. The high performance of KBS-ALC-CFAR is interpreted by detecting all existing targets and minimizing the additional false alarms.

5.3. Real Time Processing Constraints

Real-time treatment is handled for satisfying the specifications of the previous radar (PRF = 1200 HZ, $\tau = 1\,\mu s$, and antenna rotation speed = 12 rpm). On the other hand, the ADSP processor has 600 MHz which means 1.67 ns instruction cycle time. In this case, the critical time corresponds to 500,000 cycles for one pulse processing and 11,500,000 cycles for non-coherent pulse integration processing.

The execution time was computed for KBS-Dynamic-CFAR and KBS-ALC-CFAR algorithms of 800 cells and various values of N. Results obtained are presented in Fig. 18 and Fig. 19.

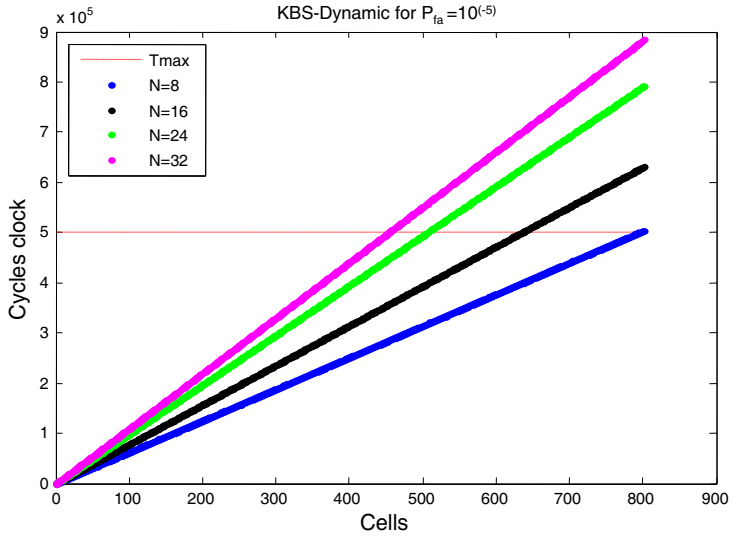

Figure 18. Execution time of KBS-Dynamic-CFAR.

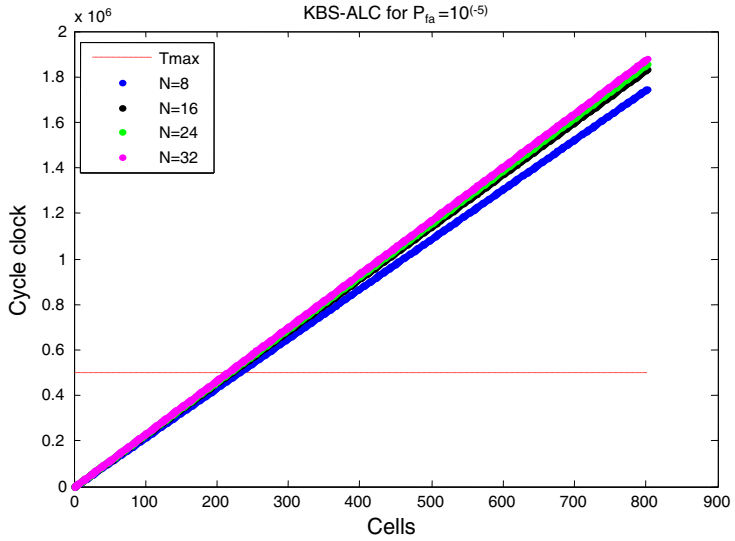

Figure 19. Execution time of KBS-ALC-CFAR.

From these simulations, we can note that the execution time of the KBS-ALC-CFAR detector is largely superior to that of KBS-Dynamic-CFAR, and this is due to the operations' nature carried out by both the detectors to calculate the detection threshold.

It can be seen that for the two detectors that the real time constraint imposed by the ASR-12 radar is not met for all values of N, because the total treatment time of all the samples exceeds 500,000

cycles critical time of a real-time application for the ASR-12 radar. One of the proposed ways to meet the ASR-12 radar's real-time requirement is to advance to a coherent integration of the pulses.

6. CONCLUSION

The proposed approach in this work aims to design a Knowledge Based Systems, KBS, that has a prior knowledge about the environment in radar detection. The new KB, called CEKB, has the advantages of high precision of the GIS and the ability of the M-N clutter edge detector to locate a possible clutter edge present in a sliding window to update the radar returns.

The principle of KBS techniques consists in choosing among the cells of the reference window, which are similar to the CUT to calculate the detection threshold.

The KBS techniques based on CEKB prove their performances to preserve its P_{fa} at the desired value, adapt to the clutter edge presence, minimize the additional false alarms, and thus remove the problem of the non-homogeneity of the environment for allowing applying ML-CFAR and Log-t-CFAR in its favorable conditions.

Considering the GIS as a KB, a comparative study shows the superiority of the new proposed architecture called KBS-FAOSOS-CFAR compared with KBS-ALC-CFAR to detect severe interference located in reference cells that have a GIS similar to the CUT.

A comparative study based on simulation and implementation results shows the outperforming of CFAR detectors that have prior knowledge about the environment compared to those that do not have any prior knowledge.

An implementation on the ADSP board of both; classical detectors and KBS detectors, shows the feasibility of these detectors and confirms the superiority of KBS detectors in terms of improving and enhancing detection performances of nonhomogeneous Weibull clutter.

As a perspective, we can make many suggestions to extend the current work:

Evaluation of the mathematical forms of the effective Pd and Pfa of the proposed architectures; KBS-ML, KBS-Log-t, and KBS-FAOSOS-CFAR.

Extend the sources of knowledge on the environment by using other knowledge based on Goodness of Fit (GoF) testing (Anderson-Darling test, Kolmogorov-Smirnov test, etc.)

In this work, we have considered the clutter model which follows the Weibull distribution; however, it can be envisaged to suppose other distributions such as K-distribution, Pareto, ... as a descriptive model under investigation.

We have assumed in this study that the clutter follows a known distribution, Weibull, we will consider in next future work that it is unknown, and we will identify it using PDF estimation methods. This makes the radar detection system based on Double Knowledge Base (DKB); Knowledge of the PDF and Knowledge of homogeneity in the reference window, which allows us to apply the appropriate CFAR detector.

APPENDIX A.

The Appendix is aimed to improve the readability. The following Table A1 summarizes the acronyms mentioned in the paper and their designations.

Table A1. List of acronyms.

Acronyms	Designations
CFAR	Constant False Alarm Rate
CEKB	Combined Environmental Knowledge Base
KBS	Knowledge Based Systems
KBS-ML-CFAR	KBS-Maximum likelihood-CFAR
GIS	Geographic Information System
KB	Knowledge Base
GLRT	Generalized Likelihood Ratio Test
MIS	Maximal Invariant Statistic
UMP	Uniformly Most Powerful
LRT	Likelihood Ratio Test
KBS-FAOSOS-CFAR	KBS-Forward Automatic Order Selection Ordered Statistics-CFAR
P_{fa}	Probability of false alarm
KBS-ALC-CFAR	KBS-Adaptive Linear Combined-CFAR
ADSP	Advanced Digital Signal Processor
PPI	Plan Position Indicator
IID	Independent and Identically Distributed
CUT	Cell Under Test
HRCS	Homogeneous Reference Cells Selector
DEKB	Dynamic update of Environmental Knowledge Base
SEKB	Static Environmental Knowledge Base
PDF	Probability Density Function
ML-CFAR	Maximum Likelihood-CFAR
CA-CFAR	Cell Averaging-CFAR
OS-CFAR	Ordered Statistic-CFAR
CCR	Clutter to Clutter Ratio
GO-CFAR	Greatest Of-CFAR
SO-CFAR	Smallest Of-CFAR
ITC	Information Theoretic Criterion
AIC	Akaike Information Criterion
MDL	Minimum Description Length
STD	Standard Deviation
PRF	Pulse Repetition Frequency
PRT	Pulse Repetition Time
RPM	Rotation Per Minute
DKB	Double Knowledge Base
N_s	Number of Samples
GoF	Goodness of Fit

REFERENCES

1. Finn, H. M., "Adaptive detection mode with threshold control as a function of spatially sampled clutter-level estimates," *RCA Rev.*, Vol. 29, 414–465, 1968.
2. Conte, E., A. De Maio, and C. Galdi, "Statistical analysis of real clutter at different range resolutions," *IEEE Transactions on Aerospace and Electronic Systems*, Vol. 40, No. 3, 903–918, 2004.

3. Hong, S. W. and D. S. Han, "Performance analysis of an environmental adaptive CFAR detector," *Mathematical Problems in Engineering*, Vol. 2014, 2014.
4. Kononov, A. A., J.-H. Kim, J.-K. Kim, and G. Kim, "A new class of adaptive CFAR methods for nonhomogeneous environments," *Progress In Electromagnetics Research B*, Vol. 64, 145–170, 2015.
5. Zaimbashi, A., "An adaptive cell averaging-based CFAR detector for interfering targets and clutter-edge situations," *Digital Signal Processing*, Vol. 31, 59–68, 2014.
6. Abbadi, A., H. Bouhedjeur, A. Bellabas, T. Menni, and F. Soltani, "Generalized closed-form expressions for CFAR detection in heterogeneous environment," *IEEE Geoscience and Remote Sensing Letters*, Vol. 15, No. 7, 1011–1015, 2018.
7. Zhang, X., R. Zhang, W. Sheng, X. Ma, Y. Han, J. Cui, and F. Kong, "Intelligent CFAR detector for non-homogeneous weibull clutter environment based on skewness," *IEEE Radar Conference (RadarConf 18)*, 0322–0326, 2018.
8. Kamal, M. S. and J. Abdullah, "New algorithm for multi targets detection in clutter edge radar environments," *Indonesian Journal of Electrical Engineering and Computer Science*, Vol. 18, No. 1, 420–427, 2020.
9. Bandiera, F., O. Besson, D. Orlando, G. Ricci, and L. L. Scharf, "GLRT-based direction detectors in homogeneous noise and subspace interference," *IEEE Transactions on Signal Processing*, Vol. 55, No. 6, 2386–2394, 2007.
10. Ciuonzo, D., A. De Maio, and D. Orlando, "A unifying framework for adaptive radar detection in homogeneous plus structured interference — Part II: Detectors design," *IEEE Transactions on Signal Processing*, Vol. 64, No. 11, 2907–2919, 2016.
11. Ciuonzo, D., A. De Maio, and P. S. Rossi, "A systematic framework for composite hypothesis testing of independent Bernoulli trials," *IEEE Signal Processing Letters*, Vol. 22, No. 9, 1249–1253, 2015.
12. Jiang, W., Y. Huang, G. Cui, and J. Yang, "Positive definite matrix space based detector with limited training samples for multiple target situations," *Progress In Electromagnetics Research M*, Vol. 60, 141–156, 2017.
13. Skolnik, M. I., *Introduction to Radar Systems*, McGraw-Hill, New York, 2001.
14. Farina, A. and F. A. Studer, "A review of CFAR detection techniques in radar systems," *Microwave Journal*, Vol. 29, 115, 1986.
15. Trunk, G. V., "Radar properties of non-Rayleigh sea clutter," *IEEE Transactions on Aerospace and Electronic Systems*, Vol. 8, No. 2, 196–204, 1972.
16. Ward, K. D., "Compound representation of high resolution sea clutter," *Electronics Letters*, Vol. 17, No. 16, 561–563, 1981.
17. Chan, H. C., "Radar sea-clutter at low grazing angles," *IEE Proceedings F — Radar and Signal Processing*, Vol. 137, No. 2, 102–112, 1990.
18. De Maio, A., A. Farina, and G. Foglia, "Knowledge-aided Bayesian radar detectors & their application to live data," *IEEE Transactions on Aerospace and Electronic Systems*, Vol. 46, No. 1, 170–183, 2010.
19. Sekine, M., Y. Mao, and Y. H. Mao, *Weibull Radar Clutter*, IET, 1990.
20. Hongsen, X. and Z. Kun, "CFAR detector using GIS information," *2010 Second IITA International Conference on Geoscience and Remote Sensing*, Vol. 2, 272–274, 2010.
21. Pourmottaghi, A., M. R. Taban, and S. Gazor, "A CFAR detector in a nonhomogenous Weibull clutter," *IEEE Transactions on Aerospace and Electronic Systems*, Vol. 48, No. 2, 1747–1758, 2012.
22. Kong, L., X. Y. Peng, and T. Zhang, "A homogenous reference cells selector for CFAR detector in highly heterogeneous environment," *Progress In Electromagnetics Research C*, Vol. 41, 175–188, 2013.
23. Song, H., S. Lu, W. Yi, and L. Kong, "CFAR detector based on clutter partition in heterogeneous background," *2015 IEEE China Summit and International Conference on Signal and Information Processing (ChinaSIP)*, 288–291, 2015.

24. Lu, S., W. Yi, G. Cui, L. Kong, and X. Yang, "Design and application of dynamic environmental knowledge base," *IET Radar, Sonar & Navigation*, Vol. 10, No. 16, 1118–1126, 2016.
25. Lu, S., W. Yi, W. Liu, G. Cui, L. Kong, and X. Yang, "Data-dependent clustering-CFAR detector in heterogeneous environment," *IEEE Transactions on Aerospace and Electronic Systems*, Vol. 54, No. 1, 476–485, 2017.
26. Darrah, C. A. and D. W. Luke, "Site-specific clutter modeling using DMA digital terrain elevation data (DTED), digital feature analysis data (DFAD), and Lincoln Laboratory five frequency clutter amplitude data," *Proceedings of the 1996 IEEE National Radar Conference*, 178–183, 1996.
27. Kurekin, A., D. Radford, K. Lever, D. Marshall, and L. K. Shark, "New method for generating site-specific clutter map for land-based radar by using multimodal remote-sensing images and digital terrain data," *IET Radar, Sonar & Navigation*, Vol. 5, No. 3, 374–388, 2011.
28. Guerci, J. R. and E. J. Baranoski, "Knowledge-aided adaptive radar at DARPA: An overview," *IEEE Signal Processing Magazine*, Vol. 23, No. 1, 41–50, 2006.
29. Marconcini, M., T. Esch, A. Felbier, and W. Heldens, "High-resolution global monitoring of urban settlements," *Proc. of REAL CORP*, 1–5, 2013.
30. Goldstein, G. B., "False-alarm regulation in log-normal and Weibull clutter," *IEEE Transactions on Aerospace and Electronic Systems*, Vol. 9, No. 1, 84–92, 1973.
31. Ravid, R. A. F. I. and N. A. D. A. V. Levanon, "Maximum-likelihood CFAR for Weibull background," *IEE Proceedings F — Radar and Signal Processing*, Vol. 139, No. 3, 256–264, 1992.
32. Weiss, M., "Analysis of some modified cell-averaging CFAR processors in multiple-target situations," *IEEE Transactions on Aerospace and Electronic Systems*, Vol. 18, No. 1, 102–114, 1982.
33. Rohling, H., "Radar CFAR thresholding in clutter and multiple target situations," *IEEE Transactions on Aerospace and Electronic Systems*, Vol. 19, No. 4, 608–621, 1983.
34. Hansen, V. G. and J. H. Sawyers, "Detectability loss due to "Greatest Of" selection in a cell-averaging CFAR," *IEEE Transactions on Aerospace and Electronic Systems*, Vol. 16, No. 1, 115–118, 1980.
35. De Maio, A., A. Farina, and G. Foglia, "Design and experimental validation of knowledge-based constant false alarm rate detectors," *IET Radar, Sonar & Navigation*, Vol. 1, No. 4, 308–316, 2007.
36. Rouabah, A., H. Zeraoula, M. H. Hamadouche, and K. Tourche, "Proposal for a radar detection architecture based on the knowledge based systems exploitation," *International Conference on Electrical Engineering and Control Applications*, 1047–1060, 2019.
37. Magaz, B., A. Belouchrani, and M. Hamadouche, "A new adaptive linear combined CFAR detector in presence of interfering targets," *Progress In Electromagnetics Research B*, Vol. 34, 367–387, 2011.
38. Magaz, B., A. Belouchrani, and M. Hamadouche, "Automatic threshold selection in OS-CFAR radar detection using information theoretic criteria," *Progress In Electromagnetics Research B*, Vol. 30, 157–175, 2011.
39. Gandhi, P. P. and S. A. Kassam, "Analysis of CFAR processors in nonhomogeneous background," *IEEE Transactions on Aerospace and Electronic Systems*, Vol. 24, No. 4, 427–445, 1988.
40. Qu, Y. and N. C. Karmakar, "Novel CFAR detection," *International Conference on Electrical and Computer Engineering*, 366–369, 2004.
41. El Mashade, M. B., "Analysis of CFAR detection of fluctuating targets," *Progress In Electromagnetics Research C*, Vol. 2, 65–94, 2008.
42. Analog Devices, "TigerSHARC embedded processors," Dec. 2006.